Earth's Future

RESEARCH ARTICLE
10.1029/2021EF002007

Key Points:

- The impact of sea level rise (SLR) on probabilistic tsunami hazard assessment (PTHA) depends on the exposure time and the relative magnitude of both phenomena
- For the probabilistic tsunami hazard assessment (PTHA) in South China Sea, the sea level rise (SLR) is as important as the uncertainty of the earthquake recurrence model
- Sea level rise (SLR) can change the tsunami propagation properties so probabilistic tsunami hazard assessment (PTHA) must include nonlinear effects in the tsunami behavior and inundation level

Supporting Information:

Supporting Information may be found in the online version of this article.

Correspondence to:

I. Sepúlveda,
sepulveda@ucsd.edu

Citation:

Sepúlveda, I., Haase, J. S., Liu, P. L.-F., Grigoriu, M., & Winckler, P. (2021). Non-stationary probabilistic tsunami hazard assessments incorporating climate-change-driven sea level rise. *Earth's Future*, *9*, e2021EF002007. https://doi.org/10.1029/2021EF002007

Received 27 JAN 2021
Accepted 15 MAY 2021

Non-Stationary Probabilistic Tsunami Hazard Assessments Incorporating Climate-Change-Driven Sea Level Rise

Ignacio Sepúlveda[1,2], Jennifer S. Haase[1], Philip L.-F. Liu[2,3,4], Mircea Grigoriu[2], and Patricio Winckler[5,6,7]

[1]Institute of Geophysics and Planetary Physics, Scripps Institution of Oceanography, University of University, San Diego, CA, USA, [2]Civil and Environmental Engineering, Cornell University, Ithaca, NY, USA, [3]Institute of Hydrological and Oceanic Sciences, National Central University in Taiwan, Taoyuan, Taiwan, [4]Department of Civil and Environmental Engineering, National University of Singapore, Singapore, [5]Escuela de Ingeniería Civil Oceánica, Universidad de Valparaíso, Valpara, Chile, [6]Centro de Investigación para la Gestión Integrada del Riesgo de Desastres, Chile, [7]Centro de Observación Marino para Estudios de Riesgos del Ambiente Corstero, Chile

Abstract We face a new era in the assessment of multiple natural hazards whose statistics are becoming alarmingly non-stationary due to ubiquitous long-term changes in climate. One particular case is tsunami hazard affected by climate-change-driven sea level rise (SLR). A traditional tsunami hazard assessment approach where SLR is omitted or included as a constant sea-level offset in a probabilistic calculation may misrepresent the impacts of climate-change. In this paper, a general method called non-stationary probabilistic tsunami hazard assessment (nPTHA), is developed to include the long-term time-varying changes in mean sea level. The nPTHA is based on a non-stationary Poisson process model, which takes advantage of the independence of arrivals within non-overlapping time-intervals to specify a temporally varying hazard mean recurrence rate, affected by SLR. The nPTHA is applied to the South China Sea (SCS) for tsunamis generated by earthquakes in the Manila Subduction Zone. The method provides unique and comprehensive results for inundation hazard, combining tsunami and SLR at a specific location over a given exposure time. The results show that in the SCS, SLR has a significant impact when its amplitude is comparable to that of tsunamis with moderate probability of exceedance. The SLR and its associated uncertainty produce an impact on nPTHA results comparable to that caused by the uncertainty in the earthquake recurrence model. These findings are site-specific and must be analyzed for different regions. The proposed methodology, however, is sufficiently general to include other non-stationary phenomena and can be exploited for other hazards affected by SLR.

Plain Language Summary Assessing natural hazards that are made worse by climate change cannot use previous methods that assume that the average behavior is a good representation of the hazard. Here we show the effect of climate-change-driven sea level rise (SLR) on tsunami hazard, where the continuously increasing SLR cannot be represented by an average value. Higher sea levels produce several changes in the tsunami behavior, including an increase in the maximum tsunami water level and in the speed the tsunami propagates. We introduce a new method which incorporates the long-term time-varying changes in mean sea level. The method can be applied to other coastal hazards, such as storm surge and waves. The new method is applied to port cities in the South China Sea (SCS) for tsunamis generated by earthquakes in the Manila Subduction Zone. We determine the probability of flooding urban areas within 50 and 100 years. The hazard in SCS is significantly impacted by SLR when it rises by an amount comparable to the tsunami height for a tsunami with moderate likelihood. The effect is comparable to that caused by the estimated uncertainty in recurrence interval of the causative earthquake. These results, though, are site-specific.

1. Introduction

A common approach to evaluate the impact of natural hazards is the probabilistic hazard assessment, in which all magnitudes of possible events are considered, including extreme scenarios, each with a given probability of occurrence, and are integrated into a single measure of the hazard probability (e.g., the

probability to exceed a certain hazard parameter value within a certain number of years). For instance, the probabilistic seismic hazard assessment (PSHA), first introduced by Cornell (1968), assumes a Poisson process model and empirical attenuation relations of seismic waves with large observational uncertainties, to evaluate the probability of exceeding a certain level of ground shaking at a particular location (e.g., a certain peak ground acceleration) within a time interval of engineering relevance. This approach was then extended to probabilistic tsunami hazard assessments (PTHA) focusing on tsunamigenic earthquakes (Geist & Parsons, 2006; Grezio et al., 2017) and landslides (Geist & Lynett, 2014; Grilli et al., 2009; Lane et al., 2016; Løvholt et al., 2020). PTHA has been widely applied to understand tsunami hazards regionally and globally (Davies et al., 2018; Grezio et al., 2017; Li et al., 2016; Mori et al., 2017; Park & Cox, 2016; Williamson et al., 2020). Uncertainties in the tsunamigenic mechanism need to be included in PTHA methodologies. Geist and Dmowska (1999) and later studies, for example, showed the important role of the slip heterogeneity in tsunami hazard assessments. Sepúlveda et al. (2019) proposed a new method to incorporate uncertainties in the earthquake mechanism (i.e., earthquake slip distribution and location) into a PTHA by means of a splitting Poisson process. Most of the existing PTHA methodologies adopt stochastic approaches to model the uncertain inputs as stationary random elements, ignoring any temporal evolution of hazard statistics. Thus, questions remain on the capability of PTHA to incorporate non-stationary processes, including those related to climate change. The focus of this paper is thus to consistently incorporate the absolute climate-change-driven sea level rise (named SLR herein) into a PTHA.

SLR has become a pressing issue for coastal communities. Its prediction and the design of adaptation measures pose challenges for scientists, engineers, and policy makers (Portner et al., 2019; Sweeney & Becker, 2020). While several SLR projections have been proposed for the present and future centuries (e.g., Horton et al., 2020), the uncertainties are significant and depend greatly on how human activities will impact the climate system. The quantification of SLR uncertainties and corresponding statistical properties (e.g., probability distributions) pose further challenges. Four scenarios known as representative concentration pathways (RCP) have been proposed to account for different evolution of greenhouse gases (Portner et al., 2019; Wang et al., 2016). The SLR uncertainties remain in these scenarios due to uncertainties in many Earth system model components, which are often handled by creating ensembles of simulations.

SLR often refers to changes of the absolute mean sea level, defined as the height with respect to an absolute reference such as the International Terrestrial Reference Frame (ITRF), for example (Woodworth & Player, 2003). As far as coastal hazards are concerned, it is also practical to evaluate changes of relative sea level, defined as the sea level height with respect to a local land-based reference (e.g., a local vertical datum). Other long-term processes modifying the relative sea level act in combination with SLR. For instance, the coast may experience subsidence or uplift in tectonically active regions (e.g., Plafker & Savage, 1970). While co-seismic ground surface deformation during an earthquake can be reasonably well estimated after the fact with various models (e.g., Mansinha & Smylie, 1971; Okada, 1985), the interseismic deformation has a large uncertainty. Climate change can also indirectly drive coastal deformation. For instance, the melting of ice sheets may produce a loading reduction on the Earth's crust, causing an uplift due to elastic rebound (Jiang et al., 2010; Larsen et al., 2005). Another example is land subsidence due to excessive groundwater and gas extraction (Chaussard et al., 2013). These additional processes can be included as corrections to the effective relative SLR (or sink) in a given study area. Even if SLR is relatively well constrained, its interaction with randomly occurring hazards (e.g., tsunamis, storm surges, meteotsunamis, and coastal storms) compounds the hazards experienced at the coast. Ultimately, it will be important to address all of these hazards in combination. For the current study, however, the question of how PTHA results will be affected by SLR alone is first addressed.

Earlier studies have responded to this question by conducting PTHA with several selected and fixed sea level scenarios. Using this simple approach, Dall'Osso et al. (2014); Li et al. (2018) showed that tsunami hazards can be significantly enhanced under certain SLR scenarios, in particular when the tsunami maximum tsunami elevation is comparable to SLR. As an illustration, Figure 1 shows the combined effect of randomly generated earthquakes, and corresponding tsunamis with SLR over a given exposure time, T, for which the hazard must be assessed, for example over the lifetime of a coastal project. The random occurrence of earthquakes e_k at times T_k, produces a hazard response (e.g., expressed as inundation) H_k at a studied site. The properties of e_k and H_k are commonly related by assuming a stationary model. However, certain coastal

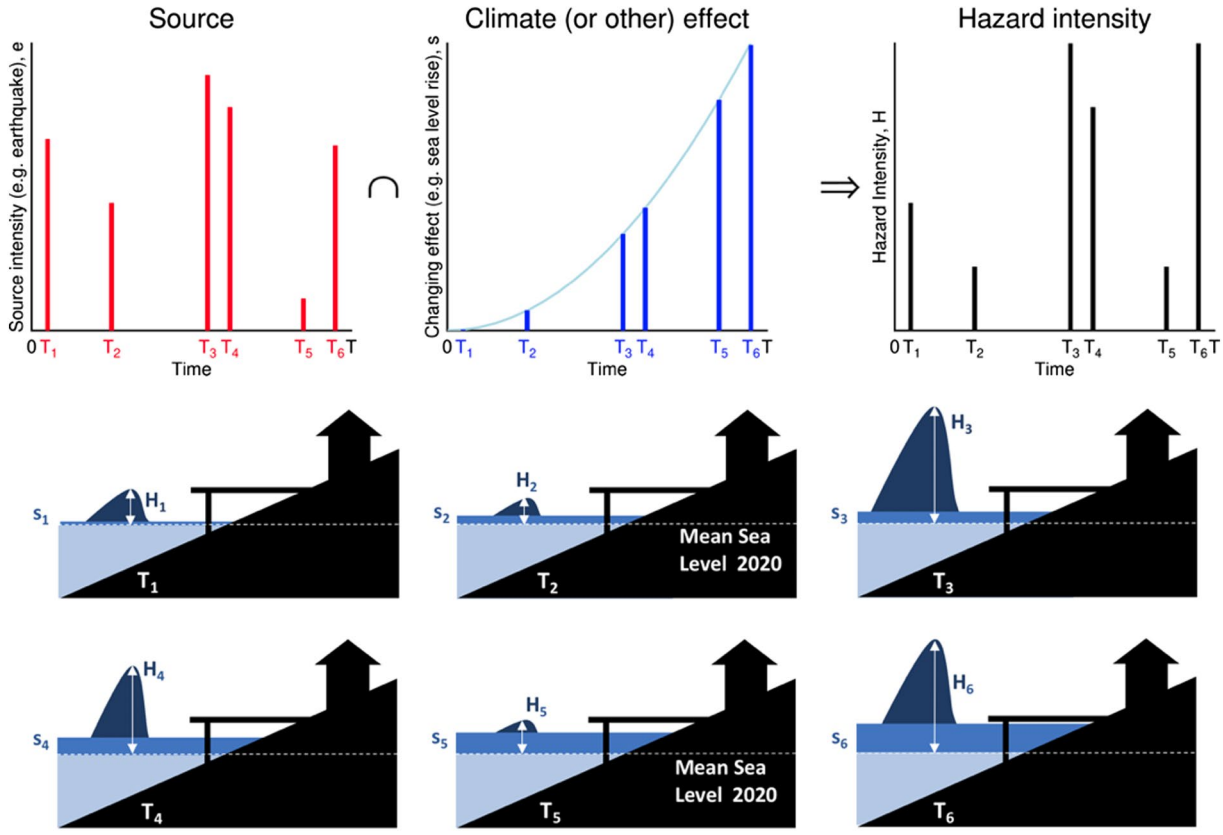

Figure 1. Top: Schematic showing the random occurrence of hazard sources e (e.g., earthquakes) at six different epochs, T_k, within an exposure time T. Some coastal hazards, such as tsunamis, will be affected by sea level rise (SLR) modifying the mean sea level $s(T_k)$. The coastal hazard response H_k (e.g., values of maximum tsunami elevation, runup, area of inundation) will result from a combination of $e(T_k)$ and $s(T_k)$. Bottom panel: Illustration of how the maximum tsunami elevation (i.e., the defined H) will be affected by the SLR at different epochs. Note the difference between tsunamis H_6 and H_1 is larger than the SLR that occurred between the two earthquakes of identical size.

hazards can be severely modified by SLR. Indeed, SLR might both increase inundation extent and change propagation depth, which in turn modifies the tsunami response. Hence, the properties of e_k in combination with the SLR at the time of occurrence of the event define H_k. The lower panel of Figure 1 shows a sketch of different earthquake events occurring in six different epochs, T_k. While the sea level is rising due to climate change, earthquakes with different characteristics (and magnitudes) generate different sizes of tsunami waves. These tsunami waves interact with the changing water depths due to SLR, generating different hazard responses, $H(T_k)$. Different mean sea levels occur at different epochs and, therefore, SLR must be included as a non-stationary process in the PTHA.

This study aims to integrate hazards occurring at random epochs (e.g., earthquakes) with a temporally evolving process (e.g., SLR) within an exposure time. In section 2 we define a general non-stationary probabilistic tsunami hazard assessment (nPTHA), based on a non-stationary Poisson process. In section 3 and 4, we apply the nPTHA in South China Sea (SCS herein), evaluating tsunamis generated in the Manila Subduction Zone and SLR projections for the 21st century. Section 5 evaluate the sensitivity of the nPTHA in the SCS to different sources of uncertainty. Finally, section 6 discusses future prospects for this new nPTHA.

2. PTHA Based on a Non-Stationary Poisson Process (nPTHA)

In Sepúlveda et al. (2019), a PTHA method was developed incorporating uncertainties in the earthquake slip distribution and location. The PTHA method sorts potential earthquakes, or any tsunamigenic source, into sets known as ensembles E_i. Earthquakes belonging to E_i have magnitudes within a defined range and originate in the same fault segment, although their location within the segment can vary. The occurrences

of earthquakes in E_i in the time interval $(0, T)$ follow a homogeneous Poisson process $N_{E_i}(T)$ with average recurrence rate $\lambda_{E_i} > 0$. The average recurrence rate is expressed in number of events per unit of time. The earthquakes belonging to E_i are independent and identically distributed random variables. Thus, $N_{E_i}(T)$ is a random number of earthquakes in $(0, T)$ with random arrival times $T_1, T_2,..., T_{N_{E_i}(T)}$. Several earthquake ensembles, which pose a tsunami hazard in the study region, are included in the PTHA and they are assumed to be independent of each other. The measures of tsunami response can be defined, for example, as the maximum tsunami elevation, the maximum current speed, the maximum flow depth, inundation extent, etc. and they are denoted by H^*. Thus, $H_1^*, H_2^*,...,H_{N_{E_i}(T)}^*$ correspond to tsunami responses caused by the $N_{E_i}(T)$ earthquakes. The responses H* are assumed to be independent and identically distributed random variables. Tsunami responses exceeding a certain value h_c are described by a new homogeneous Poisson process N_{hc} with recurrence rate $\lambda_{hc} = \lambda_{E_i} P(H^* > h_c | E_i)$, where $P(H^* > h_c|E_i)$ is the probability that H^* exceeds h_c given that an earthquake of ensemble E_i occurred. N_{hc} is referred to a thinned version of N_{E_i} (also known as the splitting of Poisson process or Raikov's Theorem (Raikov, 1938)). When including all the pertinent earthquake ensembles, the overall probability of not exceeding h_c within the time interval $(0, T)$ is given by,

$$P\left(N_{h_c}(T) = 0\right) = \prod_i e^{-\lambda_{E_i} P(H^* > h_c|E_i)T} = e^{-\lambda_S(h_c)T}, \quad (1)$$

The average recurrence rate for exceeding h_c is stationary and equal to,

$$\lambda_S(h_c) = \sum_i \lambda_{E_i} P(H^* > h_c | E_i). \quad (2)$$

The reciprocal of the average recurrence rate (i.e., $1/\lambda_S(h_c)$) is called the mean return period and is meaningful when the average recurrence rate does not change in time. Indeed, Sepúlveda et al. (2019) expressed PTHA results using mean return periods.

Let $s(t)$ be the temporal evolution (i.e., the vertical change) of the mean sea level. As the mean sea level varies with time, the probability of exceeding h_c for a certain earthquake ensemble will vary and, therefore, so will λ_{hc}. Thus, $\lambda_{hc}(t)$ should be a function of time, that is, for higher sea levels more events exceeding h_c are expected. The tsunami responses are now affected by $s(t)$ and denoted by H. Thus, $H_1, H_2,...,H_{N_{E_i}(T)}$ correspond to the tsunami responses caused by the $N_{E_i}(T)$ earthquakes and when the mean sea level is s_1, s_2,..., $s_{N_{E_i}(T)}$. Consider a partition of $(0, T)$ into m non-overlapped sub-intervals Δt, sufficiently small such that the probability of having two or more tsunamis exceeding h_c in Δt is nearly zero. Therefore, the probability of having a tsunami event exceeding h_c during an interval $(t_k, t_k + \Delta t)$ with $t_k = k\Delta t$, $k = 1, ..., m$, is $\lambda_{E_i} P(H > h_c | E_i, s(t_k))\,\Delta t \approx 1 - e^{(-\lambda_{E_i} P(H > h_c|E_i, s(t_k)))\Delta t}$, where $P(H > h_c|E_i, s(t_k))$ is the probability that H exceeds h_c given that an earthquake of ensemble E_i occurred when the sea level was $s(t_k)$. The probability that earthquakes E_i do not create tsunamis exceeding h_c in $(0, T)$ can be viewed as a sequence of m independent Bernoulli trials with probability of success $p_k = e^{(-\lambda_{E_i} P(H > h_c|E_i, s(t_k)))\Delta t}$. Thus, the probability that h_c is not exceeded is $p_1 \cdot p_2 \cdot ... \cdot p_m$. By also incorporating different ensembles of earthquakes, the expression yields,

$$P\left(N_{h_c}(T) = 0\right) = \prod_i \prod_{k=1}^{m} e^{-\lambda_{E_i} P(H > h_c|E_i, s(t_k))\Delta t}, \quad (3)$$

where i denotes the ensemble and k denotes the sub-intervals of the partition of $(0, T)$. We hypothesize that possible temporal changes in λ_{E_i} occur over time scales much longer than the SLR evolution. Thus, we assume that λ_{E_i} does not change in time and $s(t)$ is the only non-stationary process. This assumption can be further relaxed by incorporating temporal changes in λ_{E_i}. However, this is not done in the present study. By replacing Δt with $dt \to 0$, Equation 3 yields,

$$P\left(N_{h_c}(T) = 0\right) = e^{-\sum_i \lambda_{E_i} \int_0^T P(H > h_c|E_i, s(t))dt} = e^{-\bar{\lambda}_N(h_c, T)T}. \quad (4)$$

Equation 4 is referred to as a non-stationary Poisson process with average recurrence rate,

$$\overline{\lambda}_N(h_c,T) = \sum_i \lambda_{E_i} \frac{1}{T} \int_0^T P(H > h_c \mid E_i, s(t))dt. \quad (5)$$

The non-stationary Poisson process has been used in previous studies to describe the random occurrence of other types of non-stationary natural hazards (e.g., Araya & Der Kiureghian, 1988) and constitutes the main model of the nPTHA of this study. The expression for the non-exceedance probability based on the non-stationary Poisson process (i.e., Equation 4) is similar to that of the probability based on the stationary Poisson process (i.e., Equation 1). The only difference between both expressions are the recurrence rates. The calculation of the nPTHA is therefore reduced to calculating the integral in Equation 5. Here, two approaches to calculate $P(H > h_c|E_i, s(t))$ are proposed and a numerical method is developed to solve Equation 5.

2.1. Surrogate Model

The exceedance curves, $P(H > h_c|E_i, s(t))$, will change with SLR (and time). Thus, the exceedance curves built for traditional PTHA (e.g., Figure 10 in Sepúlveda et al., 2019) are not valid for this situation. The computation of $P(H > h_c|E_i, s(t))$ for continuous or very closely spaced intervals of time, t, is not feasible. For example, for a single case in Sepúlveda et al. (2019) (i.e., without SLR), a total of 640 h (27 days) were needed to compute the exceedance curves on a conventional computer (2.6 Ghz Intel quad-core i7 processor computer). We propose to determine $P(H > h_c|E_i, s(t))$ at a small number of defined epochs, called collocation epochs. This approach is called a surrogate model.

We generate n different sets of exceedance curves, $P(H > h_c|E_i, s(t_j))$, with a given sea level offset relative to the current mean sea level, $s(t_j), j = 1, .., n$, where t_j are the collocation epochs. The introduction of this offset in mean sea level is straightforward in most tsunami propagation models. In COMCOT (Wang, 2009), for instance, an offset can be specified to the mean sea level in the input information. In this study, we divide the total sea level offset at the exposure time T, $s(T)$, into n equal increments, and thus,

$$\vec{s} = [s(0), s(T)/n, 2s(T)/n, \ldots, s(T)] = [s_0, s_1, s_2, \ldots, s_n] \quad (6)$$

While the equidistant $\vec{s}$ is a valid set, the optimal one commonly depends on $P(H > h_c|E_i, s(t))$, $s(t)$ and the selected surrogate model. The set of exceedance curves with $s(0)$ is the same as that of the PTHA without SLR.

In the surrogate model, the estimation of $P(H > h_c|E_i, s(t))$ results from an interpolation of the exceedance curves $P(H > h_c|E_i, s(t_{j-1}))$ and $P(H > h_c|E_i, s(t_j))$, where $t_{j-1} < t < t_j$. To build the curve $P(H > h_c|E_i, s(t))$, we interpolate for h_c in terms of a fixed value of probability. With this interpolation, we avoid spurious results where the collocation curves reach probability of one (the maximum). The surrogate model is sufficiently general to calculate the exceedance curves of other hazard measures, such as current speeds, flow depths and inundation. The accuracy of the surrogate model depends on the number of collocation epochs, n, and should be examined and determined for each specific problem.

2.2. Linear Approximation for Maximum Tsunami Elevation

A simpler approach can be adopted to estimate $P(H > h_c|E_i, s(t))$ if two conditions are fulfilled. First, this PTHA analyzes the maximum tsunami elevation or any other measure related to the surface elevation. Second, the maximum tsunami elevation relative to the mean sea level at the time of the earthquake (i.e., the level including SLR) is independent of the value of $s(t)$. Consequently, SLR can be simply linearly superimposed on the maximum tsunami elevation resulting from a tsunami simulation without SLR, as an offset. The exceedance probability curves, $P(H > h_c|E_i)$, built for h_c in a PTHA without SLR can be easily modified by adding $s(t)$ to h_c and preserving the probability values (i.e., shifting the maximum tsunami elevation in the exceedance probability curves). With this approach we do not need to carry out additional simulations beyond those for the conventional PTHA. The validity of the linear superposition assumption, though, needs to be examined for every case study. A few tsunami simulations using the greatest earthquakes, for

example, may provide insights into the relevance of non-linear interactions. This approach is not used in this paper but it may be useful for other case studies, for example when assessing tsunamis at offshore locations.

2.3. Numerical Integration of $\int_0^T P(H > h_c \mid E_i, s(t))dt$

After using either the surrogate model or the linear superposition approach, $\int_0^T P(H > h_c \mid E_i, s(t))dt$ in Equation 5 can be computed using a trapezoidal quadrature, which uses the calculated $P(H > h_c|E_i,\ s(t))$. For instance, we select a temporally equidistant set with q + 1 elements, $\overrightarrow{s_Q} = [s(0), s(T\ /\ q), s(2T\ /\ q),\ldots,s(T)] = [s_0, s_1, s_2,\ldots,s_q]$,

$$\overline{\lambda}_N(h_c,T) = \sum_i \lambda_{E_i} \frac{1}{q}\left(\frac{P(H > h_c \mid E_i,s_0)}{2} + \sum_{k=2}^{q-1} P(H > h_c \mid E_i,s_k) + \frac{P(H > h_c \mid E_i,s_q)}{2}\right) \tag{7}$$

where q is the number of temporal sub-intervals for the trapezoidal quadrature. The accuracy of the estimated $\overline{\lambda}_N(h_c,T)$ depends on the width of the trapezoids and the estimator of $P(H > h_c|E_i,\ s(t))$. For the example case in section 3, we tested different values of q and the integral converges for $q = 20$.

2.4. nPTHA Results

The usual practice of reporting hazard in terms of average recurrence rate or return period (e.g., 100 or 1,000 years (Santiago-Fandiño et al., 2014; Sepúlveda et al., 2019) may be inadequate for nPTHA because the average recurrence rate changes depending on the exposure time T (i.e., recurrence rates are not stationary). Another useful and intuitive measure to describe the hazards is $P\left(N_{h_c}(T) = 0\right)$ in Equation 4 and the exceedance probability,

$$P\left(N_{h_c}(T) > 0\right) = 1 - P\left(N_{h_c}(T) = 0\right) = 1 - e^{-\overline{\lambda}_N(h_c,T)T}, \tag{8}$$

which gives the probability of exceeding a hazard threshold value at least one time within T (i.e., the complement of $P\left(N_{h_c}(T) = 0\right)$). The mean return period of the PTHA also presents issues for stationary problems (Serinaldi, 2015). For instance, a hazard with average return period of 1,000 years sounds very unlikely. However, the probability that such an event will occur at least one time in a human lifetime (i.e., $T \sim 100$ years) is $1 - e^{-100/1000} = 9.5\%$, which is perceived as a significant likelihood. Return periods of 2,500 and 10,000 years also correspond to significant probabilities for T = 100 years ($1 - e^{-100/2500} = 3.92\%$ and $1 - e^{-100/10,000} = 1.00\%$, respectively). Hence, the nPTHA results of the present study are expressed in terms of probabilities of exceedance within the exposure time T.

For sake of clarity, Figure S1 of the supporting information presents a diagram summarizing the method of this section.

3. nPTHA Illustration in the SCS

In this section we conduct a nPTHA for sites in Hong Kong, China, and Kao Hsiung, Taiwan, for tsunamis generated by earthquakes in the Manila Subduction Zone, incorporating SLR. The six locations that are studied are shown in Figure 2.

3.1. Earthquake Characteristics

In this nPTHA case, we include three sources of uncertainty for each earthquake. We incorporate uncertainties in the earthquake slip and location within the fault segment, as well as the uncertainty in the earthquake recurrence rate. These uncertainties are the same as those described in Sepúlveda et al. (2019) and they are presented again for convenience.

10.1029/2021EF002007

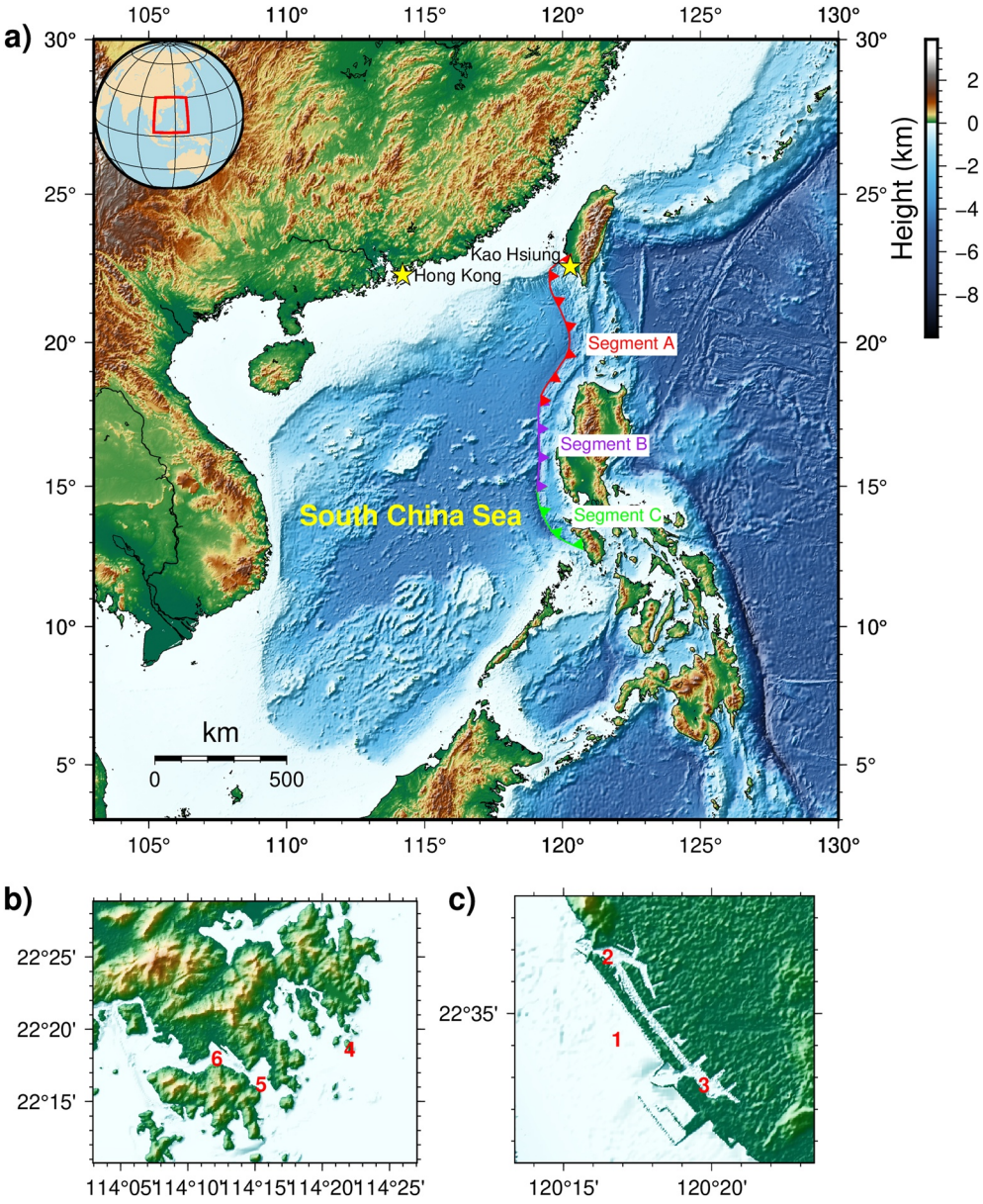

Figure 2. (a) Map of the South China Sea (SCS) and the coastal cities of Kao Hsiung, Taiwan, and Hong Kong, China. The map also shows the hypothetical fault segments (segments A, B, and C) associated with the Manila Subduction Zone. (b) Detail of bathymetry and topography in the vicinities of Hong Kong. The maximum tsunami elevation is evaluated at sites #4 Offshore Hong Kong (depth 4.17 m relative to mean sea level (MSL)), #5 East Hong Kong (depth 20.95 m MSL) and #6 West Hong Kong (in front of Kai Tak Terminal, depth 12.52 m MSL). (c) Detail of bathymetry and topography in the vicinities of Kao Hsiung. The maximum tsunami elevation is evaluated at sites #1 Offshore Kao Hsiung Port (depth 13.85 m MSL), #2 North Kao Hsiung Port (depth 8.27 m MSL) and #3 South side Kao Hsiung (inside port, depth 16.58 m MSL). Heights are relative to mean sea level in 2020.

Three seismic fault segments are analyzed. Segment A is characterized as being able to produce earthquakes with magnitude between M_W 7.5 and 9.0, segment B has the capability to produce earthquakes of magnitude between M_W 8.0 and 8.5, while segment C has the capability to produce earthquakes of magnitude M_W 8.5. The minimum earthquake magnitudes were chosen as those capable of producing significant tsunami amplitudes at the six locations of interest (i.e., the tsunami elevation with 1% probability of being exceeded is greater than 0.1 m in Hong Kong and Kao Hsiung). The maximum earthquake magnitude corresponds to the greatest earthquake that would rupture the entire length of the fault segment. The earthquake rupture

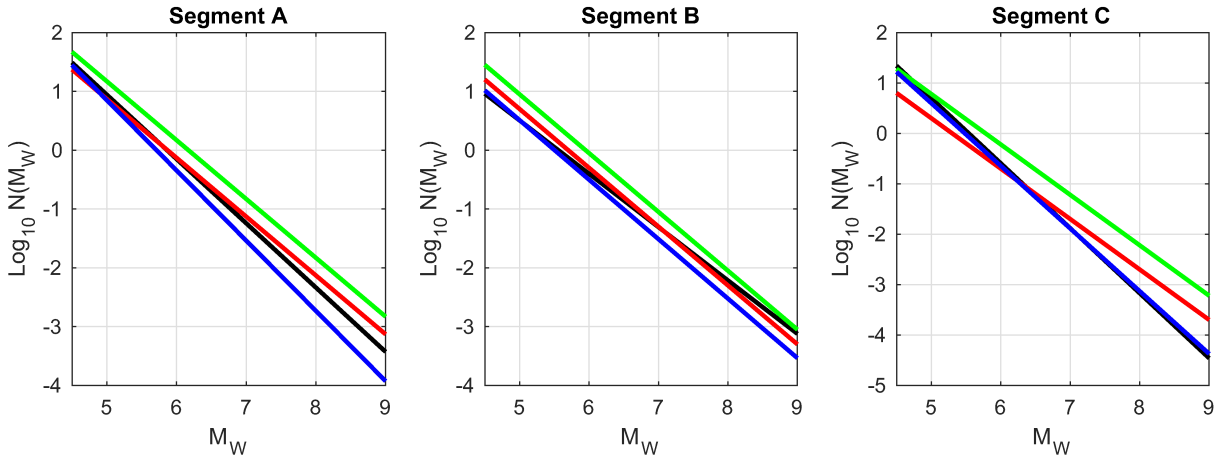

Figure 3. Empirical G-R curves of the four earthquake recurrence models used in this study. *N* represents the number of events greater than a certain magnitude per year. Black lines: Recurrence model 1. Blue lines: Recurrence model 2. Empirical recurrences are obtained from the NEIC catalog between 1974 and 2017 and use the seismogenic region limits defined in Figure S5. Green lines: recurrence model 3, using slip deficit rates of Hsu et al. (2012). Red lines: recurrence model 4, using slip deficit rates of Hsu et al. (2016). These models were elaborated in Sepúlveda et al. (2019).

area is estimated using the scaling laws of Blaser et al. (2010). The earthquake location and slip distribution are modeled as random elements using a random vector and a random field, respectively. The location is specified to be a uniformly distributed vector within each fault segment. The slip distribution is specified with a Von Karman covariance function and a Log-normal marginal distribution. We further specify the slip as a static displacement, pointing updip (pure thrust earthquakes). The slip correlation lengths and variance are estimated from the scaling laws of Raghukanth and Sangeetha (2016). The mean slip is selected to produce the target earthquake magnitude. Example of slip distributions for different target magnitudes are shown in Figures S2 and S3 of the supplemental material. Sepúlveda et al. (2019) showed that slip samples generated with a specific set of probability properties (and fixed target earthquake magnitude) have magnitudes slightly different from the target. Figure S4 of the supplemental material shows the distribution of the deviation from the target magnitude. The variability is about 0.25 magnitude units. This deviation guides the choice for discretizing the range of earthquake magnitudes. Hence, we specify target magnitudes of M_W of 9.0, 8.75, 8.5, 8.25, 8.0, 7.75, 7.5 for segment A, target magnitudes for M_W of 8.5, 8.25, and 8.0 for segment B and M_W of 8.5 for segment C. This yields 11 fault segment - magnitude bins, or ensembles, which are specified as E_1, E_2, ...E_{11}.

Sepúlveda et al. (2019) described four alternative earthquake recurrence models for the three segments of the Manila Subduction Zone. The study aimed to account for the epistemic uncertainties of the earthquake recurrence models, which can be significant in this subduction zone. The recurrence models rely on the Gutenberg Richter recurrence law (named G-R law herein), with the form $N(M_W) = 10^{a-bM_W}$, where $N(M_W)$ is the average number of earthquakes equal or greater than M_W per year, and a and b are regionally determined parameters. Two earthquake recurrence models are derived from the earthquake catalog of the USGS National Earthquake Information Center between 1974 and 2017. The historical data contains earthquakes up to M_W 7.3, the largest of which occurred in December 1999. They are used to estimate the recurrence of greater earthquakes, by means of the G-R law. Two seismogenic region sizes are used to estimate the a and b parameters for Model 1 and Model 2, which are shown in Figure S5 of the supplemental material. Two other models were derived from interseismic geodetic slip deficit rates (Hsu et al., 2012, 2016) (models 3 and 4). The G-R laws of the four recurrence models are shown in Figure 3. We also present the a and b parameters in Table S1 of the supporting information. In this section, we use the earthquake recurrence model 1 to determine the recurrence interval for a specific fault segment and magnitude bin (i.e., ensemble) λ_{E_i}. Other earthquake recurrence models are analyzed in later sections. The recurrence models proposed by Sepúlveda et al. (2019) use a simple functional form without considering a maximum earthquake magnitude. More sophisticated tapered G-R laws may provide a better representation of the recurrence. Furthermore, more than one interpretation for the Manila Subduction Zone segmentation may exist. The scarcity of geodetic

and seismic data limit the complexity of the fault source and recurrence model that can be employed. However, the differences of the four recurrence models are a reasonable attempt to account for epistemic uncertainty of the Manila Subduction Zone seismicity.

3.2. SLR Models

SLR is predicted globally based on the RCP climate scenarios, in which human activities impact global warming differently (Moss et al., 2010; Portner et al., 2019). Thus, the differences in RCP models reflect the uncertainty in human behavior rather than epistemic uncertainties of the climate models. Using the climate scenarios RCP2.6, RCP4.5 and RCP6 and RCP8.5, where RCP2.6 and RCP8.5 correspond to the lowest and highest estimated impacts, respectively, Wang et al. (2016) predicted the future SLR in the area of Macau, China, at the western side of the SCS for 2020, 2060, and 2100. Because the spatial variations are small within the SCS, as compared to the global variability (e.g., see Figure 5 of Wang et al. (2016) and Dibarboure et al. (2008)), we assume the estimated SLR values are representative of the entire SCS, and applicable to Kao Hsiung and Hong Kong. We use the predictions for 2020, 2060, and 2100 in Wang et al. (2016) to fit a quadratic curve to the sea level as a function of time,

$$s(t) = \alpha t + \beta t^2, \tag{9}$$

where α and β are calibration parameters. When $\beta > 0$, the SLR has a constant acceleration. The parameters α and β are presented in Table 1 for each RCP while the sea level projections are shown in Figure 11a. Wang et al. (2016) concluded that the SLR in SCS is ~23% larger than the global mean SLR, which is attributed to the large local thermal expansion and wind setup (i.e., wind piling up water) in the region. Hence, the SLR studied here represents a relatively large SLR case.

3.3. nPTHA for Maximum Tsunami Elevation

We determine the functions $P(H > h_c|E_i, s(t))$, where h_c is the maximum tsunami elevation at Kao Hsiung and Hong Kong (see Figures 2b and 2c). The maximum tsunami elevation is defined here as the maximum vertical distance from the still water level (without SLR) to the water surface during a tsunami. The curves $P(H > h_c|E_i, s(t))$ are built for fixed sea levels, $s(t_j)$. For each ensemble of earthquakes, we generate 200 earthquake samples with different slip distributions and locations within the fault segment. These samples are selected using a Stochastic Reduced Order Model (SROM) (Sepúlveda et al., 2017) which optimizes the accuracy of the $P(H > h_c|E_i, s(t))$ estimates. The SROM model requires the simulation of tsunamis generated by the earthquake samples. We employ the tsunami model COMCOT (Wang, 2009) solving for the non-linear shallow water equations with an explicit staggered leap-frog finite difference scheme. The model incorporates a moving boundary scheme and bottom friction using Manning's formula (with Manning coefficient 0.03 $m^{1/3}/s$). The use of COMCOT and the SROM make possible to capture the non-linear aspects of the tsunami wave propagation and the non-linear interactions with SLR. Wave non-linearity is expected to be relevant at the six locations (as well as in the inundation maps presented in the next section) because water depths are comparable to tsunami wave amplitudes. The simulated tsunami propagation, though, ignores fine scale phenomena caused by topo-bathymetry scales below the grid and data resolution (i.e., scales shorter than 45 m) and dissipation due to wave breaking. We use the same tsunami model configuration of Sepúlveda et al. (2019) consisting of nine nested grids with resolutions up to ~45 m at the six sites, where topo-bathymetry data is interpolated. The nine grids are presented in Figure S7 of the supplemental material. We further assume that the inter-seismic deformation is in balance with the co-seismic deformation over the earthquake cycle (Reid, 1911). This means that any co-seismic deformation during an earthquake will be transient and the topo-bathymetry recovers its original geometry, same as that considered as input in this study. Although there is usually some accumulated tectonic net uplift or subsidence (i.e., sculpting the local topography), it is usually much smaller than the large elastic displacement on the fault during the earthquake that is transient and mostly recovered over the earthquake cycle. For this reason, we think this is a reasonable assumption for the purpose of our simulations. The computed $P(H > h_c|E_i, s(t_j))$ curves are employed using the method of section 2.1 to estimate hazard curves at any value of $s(t)$.

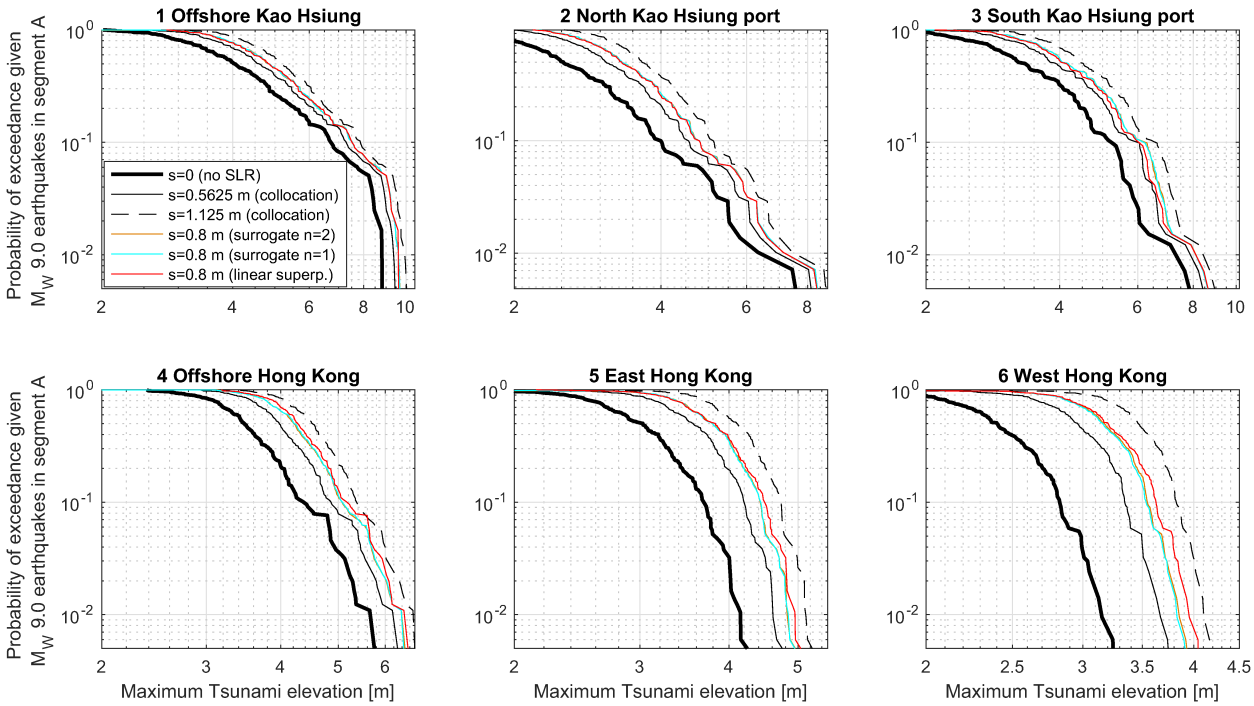

Figure 4. Examples of tsunami exceedance curves, $P(H > h_c|E_1, s)$, generated by ensemble E_1 which are defined as the set of M_W 9.0 earthquakes in Segment A of the Manila Subduction Zone. The three black curves (thick, thin, and dashed) correspond to collocation epochs where curves are explicitly calculated using fixed values of s. The cyan and orange curves correspond to estimates for $s = 0.8$ m using a surrogate model with $n = 1$ (using collocations at $s = 0$ and $s = 1.125$ m) and with $n = 2$ (using collocations at $s = 0$, $s = 0.5625$ m, and $s = 1.125$ m), respectively. The red curves correspond to the estimation for $s = 0.8$ m using the linear superposition approach.

For reference, in Figure 4 we show a comparison of $P(H > h_c|E_i, s = 0.8\text{ m})$ estimated with the surrogate model of section 2.1, different number of collocation epochs and for tsunamis generated by earthquakes with magnitude M_W 9.0 in segment A. The value of $s = 0.8$ m is arbitrarily chosen to represent a high value of s between collocation epochs. The cyan curves correspond to $n = 1$ (using collocation epochs corresponding to $s = 0$ and $s = 1.125$ m) and the orange curves correspond to $n = 2$ (using collocation epochs with $s = 0$, $s = 0.5625$, and $s = 1.125$ m). The surrogate models with $n = 1$ and $n = 2$ yield nearly identical results for this case. This comparison shows that a surrogate model with $n = 2$ achieves an acceptable accuracy. The value of n needs to be verified for each E_i and nPTHA case study. The red curves in Figure 4 also represent $P(H > h_c|E_i, 0.8\text{ m})$ estimated with the linear superposition approach of section 2.2. The greatest differences with respect to the surrogate models are found at the locations of Hong Kong and a sheltered location in Kao Hsiung (location #3). We hypothesize the larger differences at these locations are due to the inaccuracy of the linear superposition approach due to a greater contribution of non-linear interactions between the tsunami propagation and the SLR. In the results herein we adopt the surrogate model with $n = 2$. For the trapezoidal quadrature of Equation 7 we use $q = 20$. The mean sea level to which $s(t)$ is added for future epochs is defined as the mean sea level in 2020.

Figure 5 shows the average tsunami exceedance recurrence rate, $\overline{\lambda}_{N(h_c,T)}$, for given elevations h_c and for exposure times, T, of 50 years (dashed curves) and 100 years (continuous curves). The SLR model corresponds to RCP8.5 (see Table 1), which constitutes the most pessimistic of the emission scenarios analyzed in this study. Average tsunami exceedance recurrence rate curves change for different values of T, as expected. For comparison, we also plot the results of Sepúlveda et al. (2019) (i.e., PTHA without SLR) as dotted curves. For small values of maximum tsunami elevation, all curves approach the same recurrence rate, which is given by the earthquake recurrence (i.e., all values of $P(H > h_c|E_i, s)$) yield 1). The decrease of $\overline{\lambda}_{N(h_c,T)}$ at higher tsunami elevations is different depending on whether SLR is included and what T is analyzed. We use $\overline{\lambda}_{N(h_c,T)}$ to calculate the exceedance probability curves, $P\left(N_{h_c}(T) > 0\right)$, which are presented in Figure 6

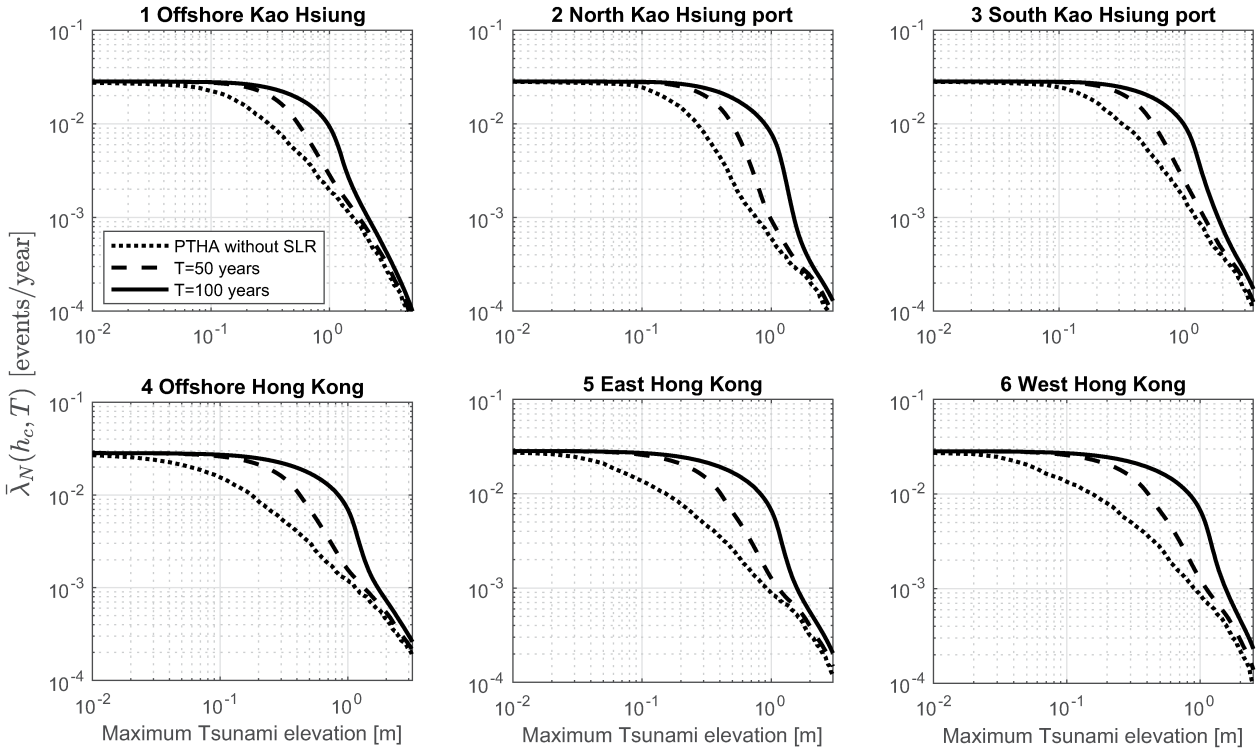

Figure 5. Average tsunami exceedance recurrence rate using a sea level rise (SLR) model based on representative concentration pathways (RCP)8.5. The dotted line corresponds to the solution of Sepúlveda et al. (2019) for earthquake recurrence model 1, without SLR. The dashed and continuous curves correspond to non-stationary probabilistic tsunami hazard assessment (nPTHA) results with SLR and with exposure times T of 50 and 100 years, respectively.

for exposure times $T = 50$ and $T = 100$ years. For reference, we plot the probabilities obtained with a PTHA without SLR as dashed lines. Small values of maximum tsunami elevation are more likely to be exceeded within the exposure time. Figure 6b shows the relative difference of the nPTHAs with respect to the results of a PTHA without SLR, expressed as the dimensionless ratio $\frac{P\left(N_{h_c}(T)>0\right)_{SLR} - P\left(N_{h_c}(T)>0\right)_{NoSLR}}{P\left(N_{h_c}(T)>0\right)_{NoSLR}}$.

A relevant finding from the comparisons between the nPTHA and PTHA is that SLR affects the maximum tsunami elevation hazard to a different degree depending on the values of h_c. We identify three intervals of h_c in $\bar{\lambda}_{N(h_c,T)}$ and $P\left(N_{h_c}(T)>0\right)$ curves with different behavior, which are described as follows. The first interval corresponds to small values of h_c where all curves overlap regardless of the value of s. Within this interval, $\bar{\lambda}_{N(h_c,T)}$ and $P\left(N_{h_c}(T)>0\right)$ curves yield a constant value. In Figure 6b this interval is present at approximately $h_c < 0.2$ m at the six locations, where differences between the nPTHA and the PTHA without SLR are small. The second interval corresponds to values of h_c greater than a threshold, in which SLR is significantly smaller than the maximum tsunami elevation. Within this interval, the nPTHAs and the PTHA without SLR produce similar estimates because the SLR impact is negligible. In Figure 6b this interval is present for $h_c > 2$ m at the six locations (i.e., s(100 years) is about half of h_c). The third and final interval is bounded by the first and second interval and is associated with the greatest differences among the nPTHAs and the PTHA without SLR. In this interval, the $\bar{\lambda}_{N(h_c,T)}$ and $P\left(N_{h_c}(T)>0\right)$ curves on a logarithmic scale have a relatively faster decay in terms of h_c $\left(\text{i.e., } \frac{d\bar{\lambda}_{N(h_c,T)}}{dh_c} \text{ and } \frac{dP\left(N_{h_c}(T)>0\right)}{dh_c}\right)$. In this interval the expected SLR and the maximum tsunami amplitude are comparable. In this case, there is a significant increase in $P\left(N_{h_c}(T)>0\right)$, compared to that of the PTHA without SLR. For $T = 100$ years, the increases for

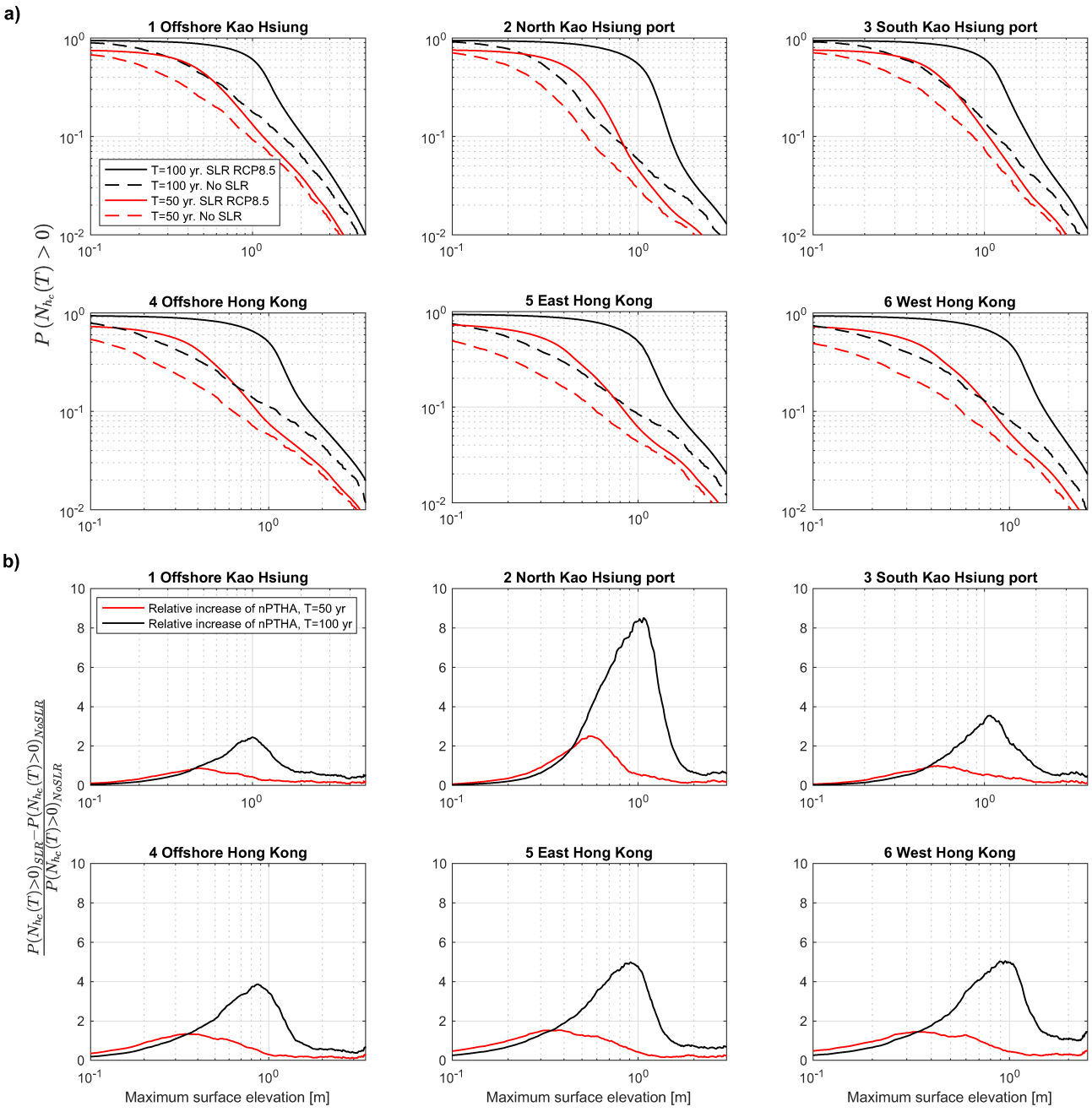

Figure 6. (a) Probability of exceedance of maximum tsunami elevation, $P\left(N_{h_c}(T)>0\right)$, incorporating sea level rise (SLR) (solid curves) for exposure times T of 50 (red) and 100 (black) years. The dashed line of same color show the probabilistic tsunami hazard assessment (PTHA) solutions without SLR. (b) Relative difference between the $P\left(N_{h_c}(T)>0\right)$ of the non-stationary probabilistic tsunami hazard assessment (nPTHA) with SLR to a PTHA without SLR, expressed as a dimensionless ratio.

the PTHA with SLR are as great as 8 times in Kao Hsiung and 5 times in Hong Kong. This result may be very different for nPTHA studies in different seismogenic regions. For nPTHA studies in nearshore locations of Japan and Chile, for example, we hypothesize that the fast decay of $P\left(N_{h_c}(T)>0\right)$ will occur for maximum tsunami elevations which are significantly higher than SLR because tsunamis and earthquakes are bigger and more frequent. Hence, we expect the relative differences between the PTHA and the nPTHA would be smaller in those cases.

4. Inundation Hazard in the SCS

The tsunami inundation hazard can also be analyzed using the surrogate model of section 2.1. Using Equation 8, the probability that the maximum tsunami elevation exceeds the topography height, Z, is expressed as,

$$P\left(N_{h_c=Z}(T) > 0\right) = 1 - e^{-\bar{\lambda}_N(h_c=Z,T)T}. \tag{10}$$

and using Equation 5 the average recurrence rate is expressed as,

$$\bar{\lambda}_N(h_c = Z,T) = \sum_i \lambda_{E_i} \frac{1}{T} \int_0^T P(H > Z \mid E_i, s(t))dt \tag{11}$$

The computation of $P(H > Z|E_i, s(t))$ at the collocation points s_j (e.g., s_0, s_1, and s_2 in the example case) is simply generated by identifying flooded and non-flooded areas in the tsunami simulations. Once $P(H > Z|E_i, s_j)$ are generated, the surrogate model and the trapezoidal quadrature are applied.

Figure 7 shows the average recurrence rate of the PTHA without SLR (panels a), the nPTHA with SLR and $T = 50$ years (panels b), and the nPTHA with SLR and $T = 100$ years (panels c). We use the SLR model from RCP8.5 and the earthquake recurrence model 1. Inundation is shown for Kao Hsiung (left) and Hong Kong (right). SLR produces a stronger impact in Hong Kong. For the case of Kao Hsiung, clearer effects are seen for $T = 100$ years at the southern end of the port.

Results for $P\left(N_{h_c=Z}(T) > 0\right)$ are calculated for T equal to 50 and 100 years. For comparison, the results of the PTHA without SLR are also calculated. Figures 8 and 9 show such results for Kao Hsiung and Hong Kong, respectively. For Hong Kong, we focus on areas with significant probability of inundation. The inundation probability is higher for $T = 100$, as expected. Again, the impact of SLR is milder for $T = 50$ years. For $T = 100$ years, conversely, the inundation probability of the nPTHA can be more than twice than that of the PTHA without SLR in some locations.

5. Sensitivity Analyses and Further Discussion

This section evaluates the relative contribution of SLR to tsunami hazard assessments compared to common sources of uncertainty. Sepúlveda et al. (2019) concluded that the earthquake recurrence model was the dominant source of uncertainty in the PTHA of SCS for earthquakes generated in the Manila Subduction Zone. Here we compare the impacts of the earthquake recurrence uncertainty on the PTHA to the effects of the SLR. The SLR projections also contain significant uncertainty which shall be further analyzed in this section. The uncertainties in the earthquake recurrence model are estimated based on using different methods commonly adopted in PTHA studies to account for epistemic uncertainties, but they are subject to the information available on seismicity rates and subduction rates. Given that the information available is limited, the true uncertainty may be higher. In other seismogenic regions where more or less comprehensive information is available to constrain recurrence rates, the sensitivity analysis may be different as well as the specific conclusions that can be drawn.

5.1. Sensitivity to Earthquake Model

The sensitivity of nPTHA results to the earthquake recurrence model will show whether the SLR is a relevant process impacting the nPTHA as compared to the dominant PTHA source of uncertainty for the study case. We produce three additional sets of nPTHA results using the earthquake recurrence models 2, 3 and 4, shown in Figure 3 and Table S1 of the supplemental material. The exposure time $T = 100$ years and the SLR model corresponding to RCP8.5 are employed.

Figure 10a shows $P\left(N_{h_c}(T) > 0\right)$ for the four earthquake recurrence models. As a reference, we plot the estimates of the PTHA using earthquake recurrence model 1 and neglecting SLR (dotted black curve).

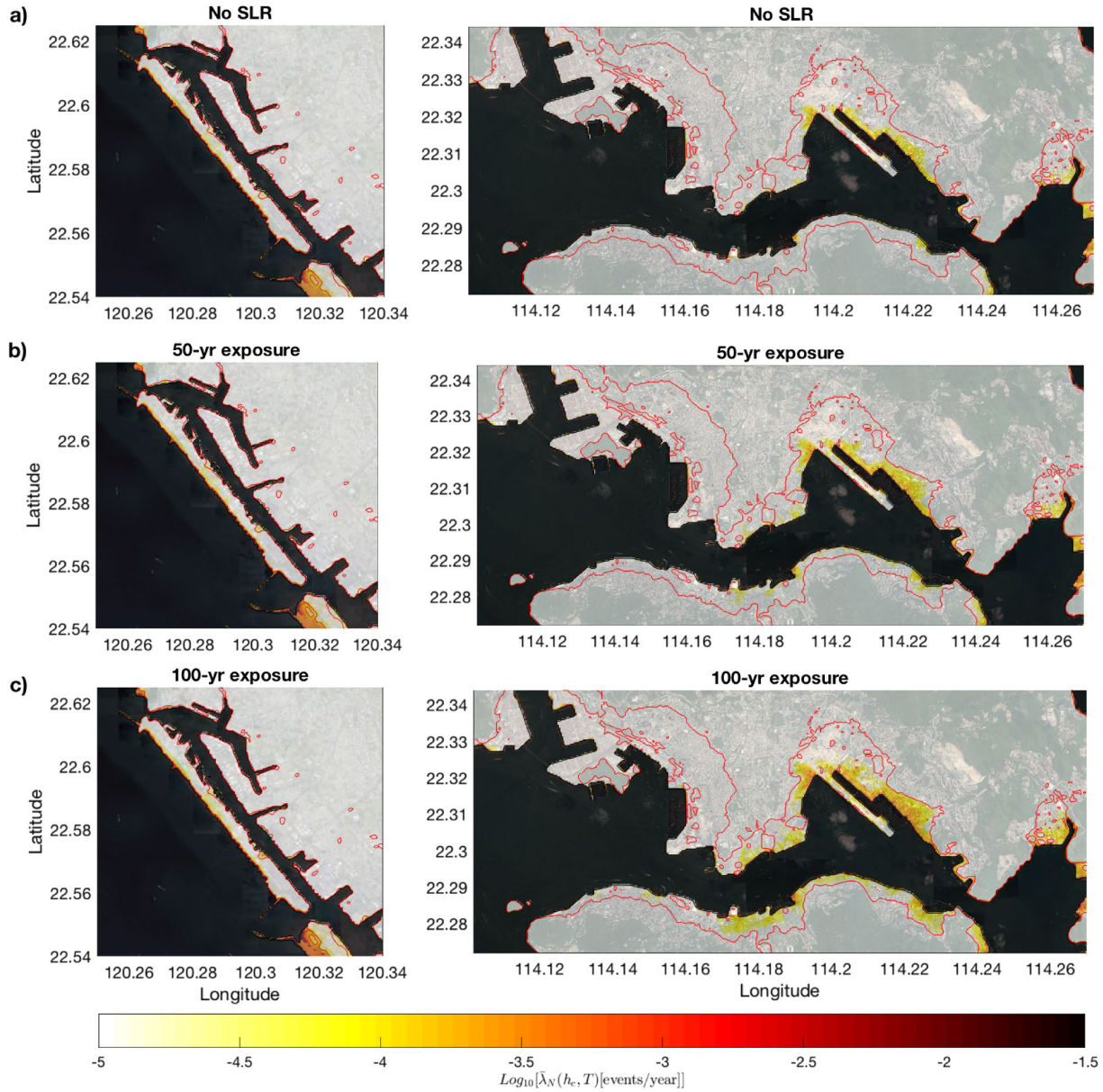

Figure 7. Average recurrence rates of inundation using: (a) a probabilistic tsunami hazard assessment (PTHA) without sea level rise (SLR), (b) a non-stationary probabilistic tsunami hazard assessment (nPTHA) with exposure time of 50 years, and (c) a nPTHA with exposure time of 100 years. The recurrence rates are presented in a logarithmic scale to show the spatial variability within the assessed regions. The red contour represents the 5 meter topography height.

Figure 10b shows the relative differences of all the nPTHA curves with respect to the PTHA using recurrence model 1 and neglecting SLR. The largest effects of SLR and earthquake recurrence model uncertainty on $P\left(N_{h_c}(T)>0\right)$ are comparable. The values of $P\left(N_{h_c}(T)>0\right)$ for earthquake recurrence model 4 with SLR are higher by as much as 15 and 10 times in Kao Hsiung and Hong Kong, respectively, as compared to the PTHA using earthquake recurrence model 1 without SLR. Because the nPTHA using earthquake recurrence model 1 with SLR is associated to an increase of $P\left(N_{h_c}(T)>0\right)$ of 8 times in Kao Hsinug and 5 times in Hong Kong, as compared to the PTHA without SLR (see section 3.2), the most conservative earthquake recurrence model 4 increases $P\left(N_{h_c}(T)>0\right)$ to about twice of that of the nPTHA with earthquake recurrence model 1. While the impact of the earthquake recurrence model seems to be somewhat smaller than the largest impact of SLR (i.e., for h_c comparable to $s(T)$), the former extends to larger values of h_c, where the

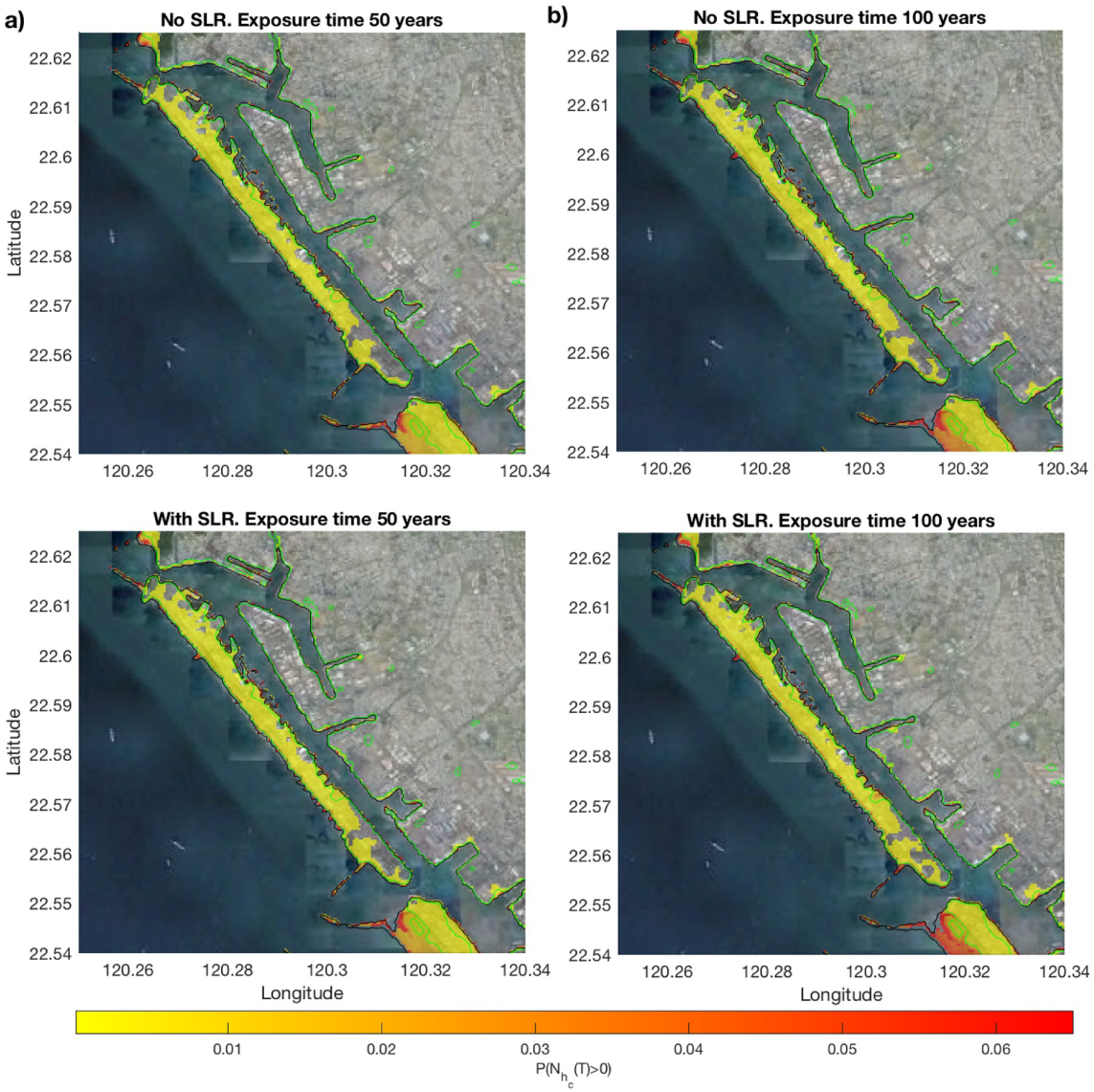

Figure 8. Probability of inundation within the exposure time T, $P\left(N_{h_c>Z}(T)>0\right)$, for the non-stationary probabilistic tsunami hazard assessment (nPTHA) with sea level rise (SLR) (lower row) and a probabilistic tsunami hazard assessment (PTHA) without SLR (top row) in Kao Hsiung for: (a) $T = 50$ and (b) $T = 100$ years. The green contour represents the 5 meter topography height. Probabilities larger than 10^{-4} are presented.

impact of SLR is smaller (i.e., where h_c is larger than $s(T)$). We conclude that the SLR produces an impact comparable to that of the earthquake recurrence model uncertainty on this nPTHA.

5.2. Sensitivity to SLR

The impacts of the less extreme pathways RCP2.6, RCP4.5, and RCP6.0 on the nPTHA are analyzed here. The earthquake recurrence model 1 and $T = 100$ years are employed. The alternative SLR projections corresponding to each RCP pathway are presented in Table 1 and shown in Figure 11a. Figure 11b presents the nPTHA results for $P\left(N_{h_c}(T)>0\right)$. All alternative RCP scenarios produce a significant impact compared to the PTHA without SLR. Figure 11c shows the relative differences of the RCP scenarios with respect to the PTHA without SLR. All maximum relative differences occur where h_c is comparable to $s(T)$. Thus, the maximum differences in $P\left(N_{h_c}(T)>0\right)$ are slightly shifted to smaller or larger h_c values depending on the

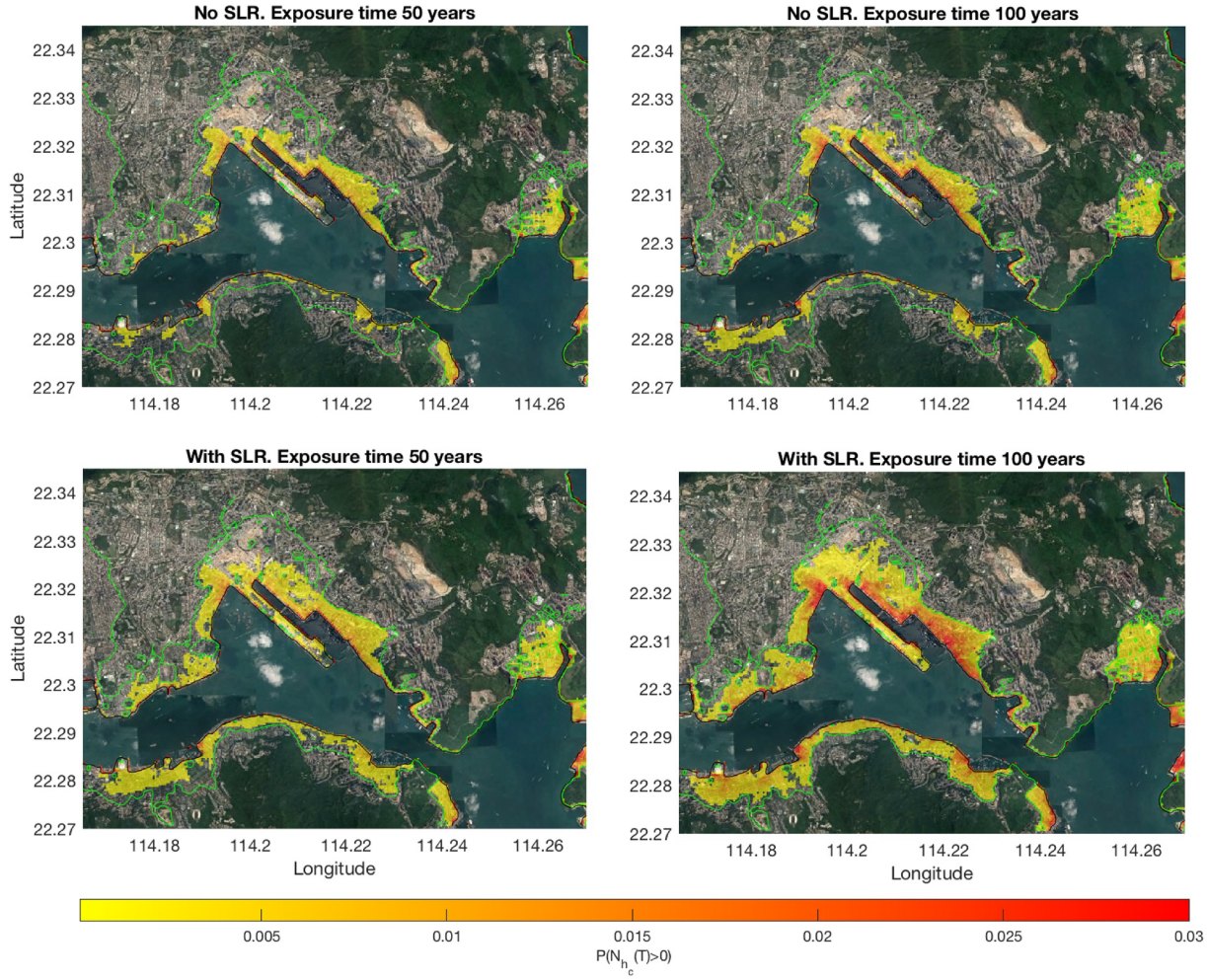

Figure 9. Probability of inundation within the exposure time T, $P\left(N_{h_c>Z}(T)>0\right)$, for the non-stationary probabilistic tsunami hazard assessment (nPTHA) with sea level rise (SLR) (lower row) and a PTHA without SLR (top row) in Hong Kong for: (a) $T = 50$ and (b) $T = 100$ years. The green contour represents the 5 meter topography height. Probabilities larger than 10^{-4} are presented.

RCP scenario. Lower RCP scenarios produce a smaller enhancement of $P\left(N_{h_c}(T)>0\right)$ as compared to the PTHA without SLR but they are still significant.

While we have evaluated the differences between the RCP scenarios, further uncertainties are present in the determination of the SLR. Such uncertainties are epistemic (i.e., due to the imperfect knowledge of the atmosphere-ocean system evolution) and difficult to quantify. Seroussi et al. (2020), for instance, illustrated the large differences between ice melting models and their contributions to SLR, from different research groups and using the same RCP scenario. As research progresses, the RCP scenarios are revised periodically in the IPCC Assessment Reports (e.g., Portner et al., 2019). Wang et al. (2016) analyzed the differences among RCP8.5 SLR predictions from 24 different models elaborated by different research groups. The reported minimum and maximum values bound the gray shaded region in Figure 11a. The difference among the models can be interpreted as a proxy of the epistemic uncertainty of the SLR prediction. We use such minimum and maximum values to determine new values of $P\left(N_{h_c}(T)>0\right)$ in Figure 11b. The nPTHA using the maximum RCP8.5 SLR predictions has significant differences as compared to that using the mean SLR prediction (black curve). For $h_c = 1$ m in location 2, for instance, the increase of $P\left(N_{h_c}(T)>0\right)$ with respect to a PTHA without SLR is ~8 and ~10 times for the mean and maximum RCP8.5 scenarios, respectively. The lowest RCP8.5 prediction is comparable to the mean SLR predictions of RCP4.5. Hence, the impact of the RCP8.5 epistemic uncertainty is comparable to that of the RCP pathways variability.

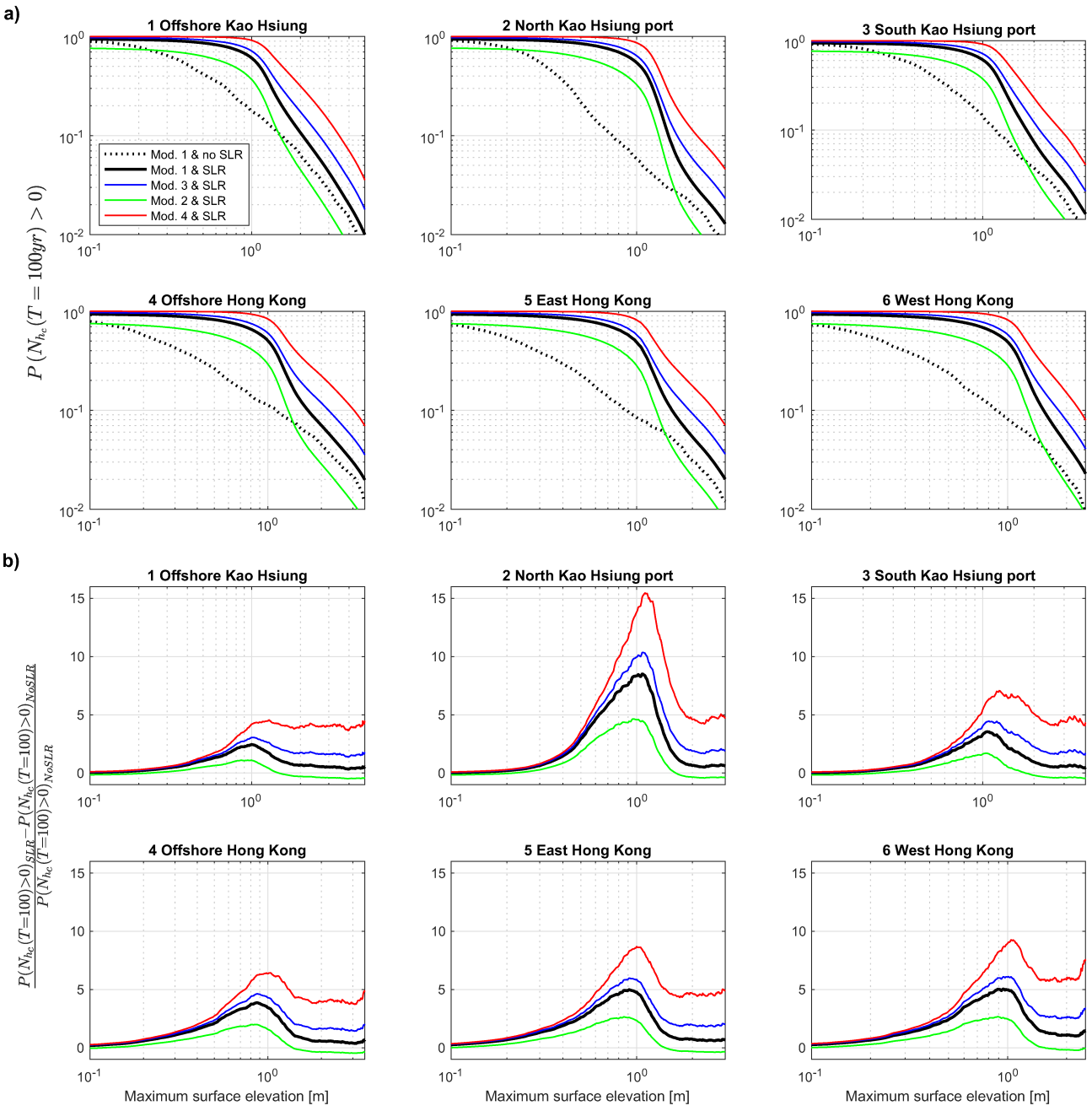

Figure 10. (a) Sensitivity analysis of non-stationary probabilistic tsunami hazard assessment (nPTHA) results $P\left(N_{h_c}(T)>0\right)$ for exposure time $T=100$ years and different earthquake recurrence models. The black, blue, green, and red curves correspond to the earthquake recurrence models 1, 2, 3, and 4, respectively, whose G-R parameters are presented in Table S1 of the supporting Information. For reference, we include $P\left(N_{h_c}(T)>0\right)$ corresponding to the PTHA without sea level rise (SLR) and using earthquake recurrence model 1 (dotted black lines). (b) Relative difference of the nPTHA results compared to the PTHA without SLR and using earthquake recurrence model 1 (dotted black curve in panel a), expressed as a dimensionless ratio.

5.3. Further Sources of Uncertainty and Discussion

Further investigation is needed to assess the accuracy of the earthquake recurrence models and the SLR projections. Additionally, other sources of uncertainty in nPTHA will require further investigation. Tides, for instance, contribute variations of amplitudes of ~1 m in Hong Kong and less than 1 m in Kao Hsiung during spring tides. Communities are often well adapted to the bounded and predicted tides. Therefore, tides alone do not constitute a hazard. However, they may exacerbate the impact of tsunami waves propagating

Table 1
α and β for the Quadratic Curve Fit in Equation 9 and Associated With the SLR Models of Wang et al. (2016)

Model	α (cm/yr)	β (cm/yr^2)
RCP2.6	0.5500	0
RCP4.5	0.5125	0.00219
RCP6.0	0.4375	0.00344
RCP8.5	0.5000	0.00625

The resulting evolution of the sea level rise (SLR), *s*, in years is presented in Figure 11.

Abbreviation: RCP, representative concentration pathways.

over a higher sea level (i.e., similar effect as SLR). Tides may be simply included as an offset of the mean sea levels in nPTHAs. For example, the nPTHA can adopt a mean sea level (as in the nPTHA above) or the average of high tides. A more sophisticated nPTHA can also include tides as a spatio-temporal random variable as the tsunami propagates. The introduction of tides as a random variable may be relevant, for example, in areas where interactions between tides and tsunamis are highly nonlinear. Winckler et al. (2017), for example, showed that tsunami-induced maximum elevations and current speeds are severely modified depending on the epoch of highly energetic tides (i.e., tide ranges >5 m and tidal currents >5 m/s). The tides shall be included in the scope of a future study.

Bathymetry may also constitute a relevant source of uncertainty in nPTHA. Recently, Sepúlveda et al. (2020) showed that altimetry-predicted bathymetry uncertainties impact the prediction of tsunami trailing waves in shallow areas. Furthermore, Kulp and Strauss (2019) showed that uncertainties of the commonly used SRTM coastal topography model can have a great impact on the prediction of relative SLR because their magnitudes are comparable. In deep waters, however, the uncertainty of bathymetry plays a minor role impacting tsunami responses (Sepúlveda et al., 2020). Indeed, Salaree and Okal (2020) showed that accurate tsunami simulations can be achieved by only analyzing the larger scale features (~1,000 km) of bathymetry in deep areas. Some other long term coastal changes may also create large impacts. The natural topo-bathymetry as well as modifications produced by human activities evolve over time. Kao Hsiung port, for instance, is experiencing a significant expansion of industrial activity and infrastructure. Thus, the topo-bathymetry model constructed in Sepúlveda et al. (2019) and used in the present study may be out-of-date in a few years. This and other long term changes, therefore, suggest that nPTHA are recommended to be updated regularly during a project design and operation.

6. Conclusions

The new nPTHA is based on a non-stationary Poisson process so that probabilistic tsunami hazards can be combined with secular effects such as SLR. Two approaches are proposed to conduct the nPTHA: (a) a surrogate model and (b) a linear superposition, which estimate probability of exceedance curves for different ensembles of earthquakes. We employed approach (a) to conduct a nPTHA at nearshore locations in the SCS, where non-linear SLR-tsunami interactions are expected to be relevant. The nPTHA method presented here may be extended to additional applications. For example, it can be used to assess the SLR impact in landslide tsunami hazard assessments, storm surge and flooding.

The results in the SCS demonstrate that SLR significantly impacts tsunami assessments for exposure times, T, as short as 50 years. The effect of the SLR is only significant when h_c, defined as the maximum tsunami elevation, is comparable to SLR within the exposure time and the probability of exceedance curve, $P\left(N_{h_c}(T) > 0\right)$, presents a significant decay in terms of h_c.

We compared the impact of SLR on the nPTHA with epistemic uncertainties in the earthquake recurrence models and SLR projection. The epistemic uncertainties are investigated with the use of alternative models. Given the limited nature of the information available in the seismicity catalog and for subduction rates in this region, the true uncertainties may be larger. Sensitivity analyses of the nPTHA in Hong Kong and Kao Hsiung demonstrate that the SLR produces an impact comparable to the earthquake recurrence model uncertainty modifying $P\left(N_{h_c}(T) > 0\right)$. The latter is identified as a major source of uncertainty in a previous PTHA study (Sepúlveda et al., 2019). The uncertainty in the SLR projections are explored in this study by varying the RCP scenarios. The chosen RCP scenarios and their estimated epistemic uncertainties can also significantly modify $P\left(N_{h_c}(T) > 0\right)$. The relative importance of the SLR versus nPTHA uncertainties is site-specific and must be analyzed for every nPTHA.

The final question is whether SLR should be included in all probabilistic tsunami hazard assessments. It is evident in the present study that the contribution of SLR is relevant in Hong Kong and Kao Hsiung.

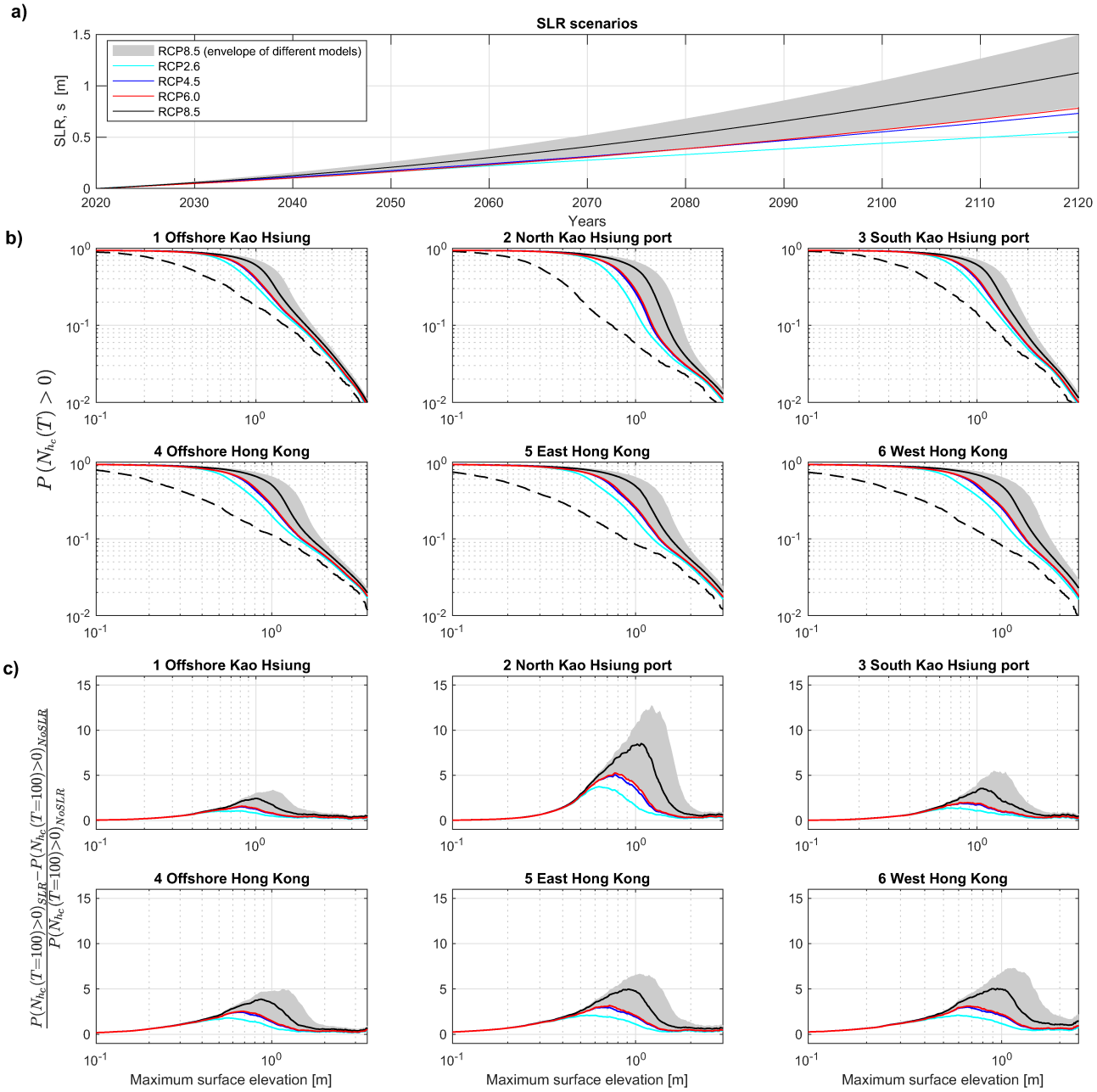

Figure 11. (a) Mean sea level rise (SLR) projections from climate model runs using representative concentration pathways (RCP)8.5 (black), RCP6.0 (red), RCP4.5 (blue) and RCP2.8 (cyan) (same of Table 1). The gray shaded region represents the variability of SLR in the South China Sea (SCS) from RCP8.5 as simulated from different models (Wang et al., 2016). (b) Sensitivity of $P\left(N_{h_c}(T)>0\right)$ to the RCP scenarios. The curves are associated with $T=100$ years and earthquake recurrence model 1. The dashed black curves represent $P\left(N_{h_c}(T)>0\right)$ of the probabilistic tsunami hazard assessments (PTHA) without SLR. (c) Relative differences of the non-stationary probabilistic tsunami hazard assessment (nPTHA) results compared to the $P\left(N_{h_c}(T)>0\right)$ of the PTHA without SLR expressed as a dimensionless ratio.

However, the relevance of the SLR in nPTHA might be different in different regions. A simple comparison between the $P\left(N_{h_c}(T)>0\right)$ curve of a PTHA without SLR–with h_c defined as the maximum tsunami elevation - and the expected SLR within T may provide preliminary insights into whether a nPTHA is necessary. If the sea level at time T, $s(T)$, and a maximum tsunami elevation of interest are similar, then the impact of SLR is expected to be relevant. In regions where tsunami waves are expected to be higher than $s(T)$ and

more frequent, in contrast, we expect a lower impact of the SLR. A nPTHA with the linear superposition approach may also provide a first approximation to assess the relevance of SLR.

Data Availability Statement

The tsunami propagation model of this paper used topo-bathymetry information obtained from the General Bathymetric Chart of the Oceans (GEBCO, available at http://www.gebco.net), SRTM topography data (available at http://earthexplorer.usgs.gov), the nautical chart of Kao Hsiung port (British Admiralty Chart 2376), nautical charts of Hong Kong (available at the official site of the Hydrographic office of the Marine Department of Hong Kong, http://www.hydro.gov.hk), Lidar data of the Civil Engineering and Development Department of Hong Kong (requested at http://www.hyd.gov.hk), and partial data from digital elevation models provided by the National Central University in Taiwan.

Acknowledgments
Tsunami simulations employed the model COMCOT and some figures were created using GMT. The authors would like to thank the Marine Department of Hong Kong, the Civil Engineering and Development Department of Hong Kong, and Dr. Tso-Ren Wu from National Central University in Taiwan for their valuable support in this and previous studies. The authors also would like to thank H. Fricker for insightful comments on the IPCC Assessment Reports and the sea level rise models. The authors also thank the valuable comments of two anonymous reviewers. I. Sepúlveda would like to acknowledge the support of the John Miles Fellowship and the Green Foundation. J. S. Haase would like to acknowledge the support of National Science Foundation Grant OAC-1835372. P. L-F. Liu would like to acknowledge the support from the National Research Foundation through a research grant to National University of Singapore and a research grant from the Earth Observatory of Singapore. P. Winckler thanks grant ANID FONDAP 15110017 (CIGIDEN) for the financial support during this study.

References

Araya, R., & Der Kiureghian, A. (1988). *Seismic hazard analysis: Improved models, uncertainties and sensitivities*, Earthquake Engineering Research Center. College of Engineering: University ÂĚ.

Blaser, L., Krüger, F., Ohrnberger, M., & Scherbaum, F. (2010). Scaling relations of earthquake source parameter estimates with special focus on subduction environment. *Bulletin of the Seismological Society of America*, *100*(6), 2914–2926. https://doi.org/10.1785/0120100111

Chaussard, E., Amelung, F., Abidin, H., & Hong, S.-H. (2013). Sinking cities in Indonesia: ALOS PALSAR detects rapid subsidence due to groundwater and gas extraction. *Remote Sensing of Environment*, *128*, 150–161. https://doi.org/10.1016/j.rse.2012.10.015

Cornell, C. A. (1968). Engineering seismic risk analysis. *Bulletin of the Seismological Society of America*, *58*(5), 1583–1606.

Dall'Osso, F., Dominey-Howes, D., Moore, C., Summerhayes, S., & Withycombe, G. (2014). The exposure of Sydney (Australia) to earthquake-generated tsunamis, storms and sea level rise: A probabilistic multi-hazard approach. *Scientific Reports*, *4*, 7401. https://doi.org/10.1038/srep07401

Davies, G., Griffin, J., Løvholt, F., Glimsdal, S., Harbitz, C., Thio, H. K., et al. (2018). A global probabilistic tsunami hazard assessment from earthquake sources. *Geological Society, London, Special Publications*, *456*(1), 219–244. https://doi.org/10.1144/sp456.5

Dibarboure, G., Lauret, O., Mertz, F., Rosmorduc, V., & Maheu, C. (2008). SSALTO/DUACS user handbook:(m) SLA and (m) ADT near-real time and delayed time products. *Rep. CLS-DOS-NT*, *6*, 39.

Geist, E. L., & Dmowska, R. (1999). Local tsunamis and distributed slip at the source. In *Seismogenic and tsunamigenic processes in shallow subduction zones* (pp. 485–512). Springer. https://doi.org/10.1007/978-3-0348-8679-6_6

Geist, E. L., & Lynett, P. J. (2014). Source processes for the probabilistic assessment of tsunami hazards. *Oceanography*, *27*(2), 86–93. https://doi.org/10.5670/oceanog.2014.43

Geist, E. L., & Parsons, T. (2006). Probabilistic analysis of tsunami hazards. *Natural Hazards*, *37*(3), 277–314. https://doi.org/10.1007/s11069-005-4646-z

Grezio, A., Babeyko, A., Baptista, M. A., Behrens, J., Costa, A., Davies, G., et al. (2017). Probabilistic tsunami hazard analysis: Multiple sources and global applications. *Reviews of Geophysics*, *55*(4), 1158–1198. https://doi.org/10.1002/2017rg000579

Grilli, S. T., Taylor, O.-D. S., Baxter, C. D. P., & Maretzki, S. (2009). A probabilistic approach for determining submarine landslide tsunami hazard along the upper east coast of the United States. *Marine Geology*, *264*(1–2), 74–97. https://doi.org/10.1016/j.margeo.2009.02.010

Horton, B. P., Khan, N. S., Cahill, N., Lee, J. S. H., Shaw, T. A., Garner, A. J., et al. (2020). Estimating global mean sea-level rise and its uncertainties by 2100 and 2300 from an expert survey. *Npj Climate and Atmospheric Science*, *3*(1), 1–8. https://doi.org/10.1038/s41612-020-0126-0

Hsu, Y.-J., Yu, S.-B., Loveless, J. P., Bacolcol, T., Solidum, R., Luis, A., et al. (2016). Interseismic deformation and moment deficit along the Manila subduction zone and the Philippine fault system. *Journal of Geophysical Research: Solid Earth*, *121*(10), 7639–7665. https://doi.org/10.1002/2016jb013082

Hsu, Y.-J., Yu, S.-B., Song, T.-R. A., & Bacolcol, T. (2012). Plate coupling along the Manila subduction zone between Taiwan and northern Luzon. *Journal of Asian Earth Sciences*, *51*, 98–108. https://doi.org/10.1016/j.jseaes.2012.01.005

Jiang, Y., Dixon, T. H., & Wdowinski, S. (2010). Accelerating uplift in the North Atlantic region as an indicator of ice loss. *Nature Geoscience*, *3*(6), 404–407. https://doi.org/10.1038/ngeo845

Kulp, S. A., & Strauss, B. H. (2019). New elevation data triple estimates of global vulnerability to sea-level rise and coastal flooding. *Nature Communications*, *10*(1), 1–12. https://doi.org/10.1038/s41467-019-12808-z

Lane, E. M., Mountjoy, J. J., Power, W. L., & Popinet, S. (2016). Initialising landslide-generated tsunamis for probabilistic tsunami hazard assessment in cook strait. *The International Journal of Ocean and Climate Systems*, *7*(1), 4–13. https://doi.org/10.1177/1759313115623162

Larsen, C. F., Motyka, R. J., Freymueller, J. T., Echelmeyer, K. A., & Ivins, E. R. (2005). Rapid viscoelastic uplift in southeast Alaska caused by post-little ice age glacial retreat. *Earth and Planetary Science Letters*, *237*(3–4), 548–560. https://doi.org/10.1016/j.epsl.2005.06.032

Li, L., Switzer, A. D., Chan, C.-H., Wang, Y., Weiss, R., & Qiu, Q. (2016). How heterogeneous coseismic slip affects regional probabilistic tsunami hazard assessment: A case study in the south china sea. *Journal of Geophysical Research: Solid Earth*, *121*(8), 6250–6272. https://doi.org/10.1002/2016jb013111

Li, L., Switzer, A. D., Wang, Y., Chan, C.-H., Qiu, Q., & Weiss, R. (2018). A modest 0.5-m rise in sea level will double the tsunami hazard in Macau. *Science advances*, *4*(8), eaat1180. https://doi.org/10.1126/sciadv.aat1180

Løvholt, F., Glimsdal, S., & Harbitz, C. B. (2020). On the landslide tsunami uncertainty and hazard. *Landslides*, *17*, 2301–2315.

Mansinha, L., & Smylie, D. E. (1971). The displacement fields of inclined faults. *Bulletin of the Seismological Society of America*, *61*(5), 1433–1440.

Mori, N., Muhammad, A., Goda, K., Yasuda, T., & Ruiz-Angulo, A. (2017). Probabilistic tsunami hazard analysis of the pacific coast of Mexico: Case study based on the 1995 Colima earthquake tsunami. *Frontiers in built environment*, *3*, 34. https://doi.org/10.3389/fbuil.2017.00034

Moss, R. H., Edmonds, J. A., Hibbard, K. A., Manning, M. R., Rose, S. K., Van Vuuren, D. P., et al. (2010). The next generation of scenarios for climate change research and assessment. *Nature*, *463*(7282), 747–756. https://doi.org/10.1038/nature08823

Okada, Y. (1985). Surface deformation due to shear and tensile faults in a half-space. *Bulletin of the Seismological Society of America*, *75*(4), 1135–1154.

Park, H., & Cox, D. T. (2016). Probabilistic assessment of near-field tsunami hazards: Inundation depth, velocity, momentum flux, arrival time, and duration applied to Seaside, Oregon. *Coastal Engineering*, *117*, 79–96. https://doi.org/10.1016/j.coastaleng.2016.07.011

Plafker, G., & Savage, J. C. (1970). Mechanism of the Chilean earthquakes of May 21 and 22, 1960. *Geological Society of America Bulletin*, *81*(4), 1001–1030. https://doi.org/10.1130/0016-7606(1970)81(1001:motceo)2.0.co;2

Portner, H. O., Roberts, D. C., Masson-Delmotte, V., Zhai, P., Tignor, M., Poloczanska, E., et al. (2019). *IPCC special report on the ocean and cryosphere in a changing climate*. Intergovernmental Panel on Climate Change.

Raghukanth, S., & Sangeetha, S. (2016). A stochastic model for earthquake slip distribution of large events. *Geomatics, Natural Hazards and Risk*, *7*(2), 493–521. https://doi.org/10.1080/19475705.2014.941418

Raikov, D. (1938). On the decomposition of Gauss and Poisson laws, *Izvestiya Rossiiskoi Akademii Nauk. Seriya Matematicheskaya*, *2*(1), 91–124.

Reid, H. F. (1911). The elastic-rebound theory of earthquakes. *California University of Department of Geology: Bulleti*, *6*(19), 413–444.

Salaree, A., & Okal, E. A. (2020). Effects of bathymetry complexity on tsunami propagation: A spherical harmonics approach. *Geophysical Journal International*, *223*(1), 632–647. https://doi.org/10.1093/gji/ggaa334

Santiago-Fandiño, V., Kontar, Y., & Kaneda, Y. (2014). *Post-tsunami hazard: Reconstruction and restoration* (Vol. 44). Springer.

Sepúlveda, I., Liu, P. L.-F., & Grigoriu, M. (2019). Probabilistic tsunami hazard assessment in south china sea with consideration of uncertain earthquake characteristics. *Journal of Geophysical Research: Solid Earth*, *124*(1), 658–688. https://doi.org/10.1029/2018jb016620

Sepúlveda, I., Liu, P. L.-F., Grigoriu, M., & Pritchard, M. (2017). Tsunami hazard assessments with consideration of uncertain earthquake slip distribution and location. *Journal of Geophysical Research: Solid Earth*, *122*(9), 7252–7271. https://doi.org/10.1002/2017jb014430

Sepúlveda, I., Tozer, B., Haase, J. S., Liu, P. L.-F., & Grigoriu, M. (2020). Modeling uncertainties of bathymetry predicted with satellite altimetry data and application to tsunami hazard assessments. *Journal of Geophysical Research: Solid Earth*, *125*, e2020JB019735. https://doi.org/10.1029/2020JB019735

Serinaldi, F. (2015). Dismissing return periods! *Stochastic environmental research and risk assessment*, *29*(4), 1179–1189. https://doi.org/10.1007/s00477-014-0916-1

Seroussi, H., Nowicki, S., Payne, A. J., Goelzer, H., Lipscomb, W. H., Abe-Ouchi, A., et al. (2020). ISMIP6 Antarctica: A multi-model ensemble of the Antarctic ice sheet evolution over the 21st century. *The Cryosphere*, *14*(9), 3033–3070.

Sweeney, B., & Becker, A. (2020). Considering future sea level change in maritime infrastructure design: A survey of US engineers. *Journal of Waterway, Port, Coastal, and Ocean Engineering*, *146*(4), 04020,019. https://doi.org/10.1061/(asce)ww.1943-5460.0000583

Wang, L., Huang, G., Zhou, W., & Chen, W. (2016). Historical change and future scenarios of sea level rise in Macau and adjacent waters. *Advances in Atmospheric Sciences*, *33*(4), 462–475. https://doi.org/10.1007/s00376-015-5047-1

Wang, X. (2009). *User manual for COMCOT version 1.7 (first draft)*. Cornell University.

Williamson, A., Rim, D., Adams, L., LeVeque, R. J., Melgar, D., & Gonzalez, F. (2020). *A source clustering approach for efficient inundation modeling and regional scale PTHA*. EarthArXiv.

Winckler, P., Sepúlveda, I., Aron, F., & Contreras-López, M. (2017). How do tides and tsunamis interact in a highly energetic channel? The case of Canal Chacao, Chile. *Journal of Geophysical Research: Oceans*, *122*, 9605–9624. https://doi.org/10.1002/2017JC012680

Woodworth, P. L., & Player, R. (2003). The permanent service for mean sea level: An update to the 21st century. *Journal of Coastal Research*, 287–295.